# Simulation Design of Power Electronic Transformer with Dual-PWM

Jiu-yang Mu[1], En Fang[1(✉)], Guan-bao Zhang[1], and Song-hai Zhou[2]

[1] School of Information and Electrical Engineering, Xuzhou University of Technology, Xuzhou 221018, Jiangsu, China
fangen@cumt.edu.cn

[2] Scientific Research Management Department, Jiangsu Zongshen Automobile Industry Limited Company, Xuzhou 221018, Jiangsu, China

**Abstract.** With the continuous development of new energy power generation and smart grid, Power Electronic Transformer (PET) has a good prospect for development because of its remarkable advantages. Based on the topology of AC/DC/AC, the modulation strategy with dual-PWM (Pulse Width Modulation) is adopted to control the operation of power electronic transformers in this paper. The PET structure is consisted of three units: input portion, isolation portion and output portion. Model building and analyzing both at the input and output terminals are achieved step by step. And the simulation of the whole PET system with dual-PWM is accomplished with MATLAB/ Simulink. The simulation results show the control system stability and output voltage regulation precision are improved with feed forward voltage decoupling vector control system. The correctness and effectiveness of the control strategy are demonstrated through the simulation. PETs play an important role in enhancing power supply reliability for Power Grid and promoting the new energy power generation development.

**Keywords:** Power electronic transformer · Topology · Loop control · Modeling simulation

## 1 Introduction

Nowadays, power distribution transformers have great application prospects with the development of distributed power generation and smart grid. The transformer is not only used to provide electrical isolation, but also to connect the system at different voltage levels. Generally, the transformer size is inversely proportional to the operating frequency. The steady reduction in the cost of power electronics and the advent of advanced magnetic materials with lower loss density and high saturation flux density proclaim that power electronic transformers with high power density design are feasible and economical.

In China, research on power electronic transformers started relatively late compared with the developed countries and is still in its infancy stage. In this paper, the output of


H. Song and D. Jiang (Eds.): SIMUtools 2020, LNICST 370, pp. 464–478, 2021.
https://doi.org/10.1007/978-3-030-72795-6_38

PET based on dual-PWM (Pulse Width Modulation) is analyzed. The dual-loop decoupling control strategy is adopted both at the input and output ends, and the dynamic response speed of the control system is improved by voltage feedforward. The intermediate isolation portion is controlled with an open-loop control strategy. Through simulation verification, the output voltage waveform can be obtained, which has a high-power quality. The voltage fluctuates with the load variation.

## 2 Circuit Structure of Dual-PWM Power Electronic Transformer

### 2.1 DC Topology in PET

In this paper, AC/DC/AC conversion structure is adopted in PETs as shown in Fig. 1. The working process is as follows: the power frequency AC input is converted into DC power on the primary side, then the DC power is inverted into high frequency alternating current. Then the high frequency alternating current is transmitted to the secondary side. The conversion process is reversed [1]. There are two AC/DC/AC converters in the power electronic transformer topology [2, 3]. With a circuit consisting of two DC bus lines (low-voltage DC bus and medium-voltage DC bus), a transformer can be used to isolate two power supplies required by certain electrical safety standards.

In the structure of the PET DC-DC converter stage, single-phase dual-active-bridge (DAB) circuit with high efficiency and few passive components is studied in this paper.

### 2.2 Overall Structure of PET

PET works at high frequencies. The size of the transformer is inversely proportional to the frequency and saturation flux density, so the size can be reduced under high-frequency operating conditions [4–6]. The active-double-bridge topology is used in DC portion of PET, so the overall structure of PET is shown in Fig. 2 [7–9].

Among many types of PET systems, AC/DC/AC transformation is chosen in this paper. As can be seen from Fig. 2, this PET type has a three-stage structure [10–12].They are input portion (three-phase voltage source type PWM rectifier), intermediate portion (DC-DC converter) and output portion (three-phase voltage source type PWM inverter). Input portion can effectively control power factor and stabilize DC voltage, energy bidirectional flow (with fully controlled devices). Intermediate portion turns high-voltage direct current into high-frequency medium-voltage direct current while achieving electrical isolation [13–15].The output portion uses a three-phase, three-wire two-level topology [16–19].

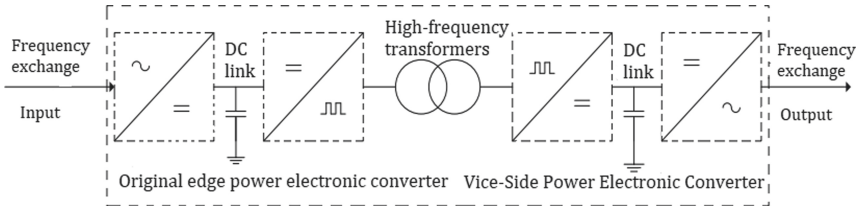


**Fig. 1.** PET with DC link.

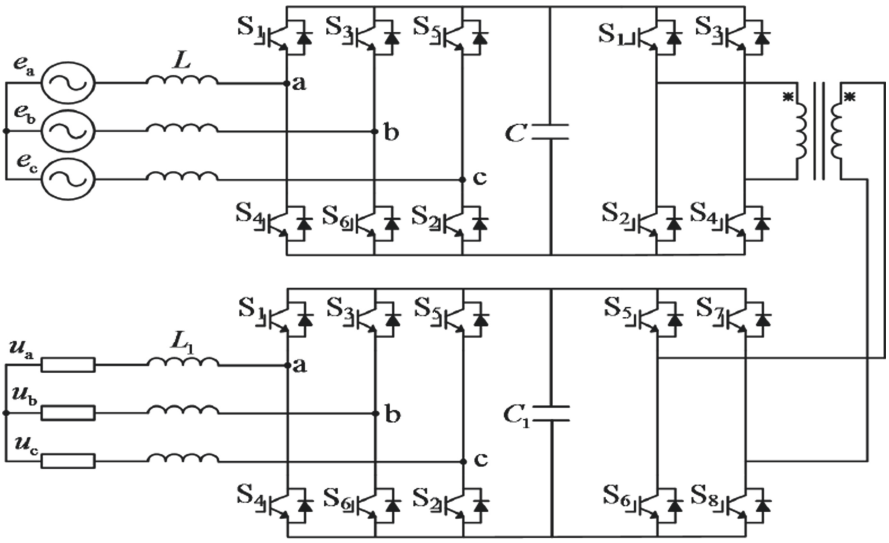


**Fig. 2.** PET overall circuit structure diagram.

## 3 Control Topology Design of Power Electronic Transformer

### 3.1 Control Topology of the PWM Converter on the Input Side

1) Control topology for the input side

On the input side, the rectification is accomplished with PWM. The space vector control topology is used in the converter oriented with the d-axis [20, 21]. The calculation formulas of active power $P$ and reactive power $Q$ in the PWM converter are as follows:

$$P = \frac{3}{2}(e_{gd}i_d + e_{gq}i_q) \tag{1}$$

$$Q = \frac{3}{2}(e_{gq}i_d - e_{gd}i_q) \tag{2}$$

Where: $P$- active power (W); $Q$- reactive power (Var); $i_d$- d-axis current component; $i_q$- q-axis current component; $e_{gd}$- d-axis current component; $e_{gq}$- q-axis current component.

As shown in Fig. 3, the active power is controlled by $i_d$ and the reactive is by $i_q$. With the help of energy balance theory, it can be expressed as follows:

$$u_{dc} i_{dc} = \frac{3}{2} e_{gd} i_d \tag{3}$$

As can be seen from Eq. (3), the active power is only related to the d-axis current component. Therefore, double-loop control topology can be adopted. As shown in Fig. 3, the outer loop is a DC voltage loop, and the inner loop is a d-axis current loop.

As shown in Fig. 3, the control process can be described as follows: the main control of the voltage outer loop is to realize the stability of the DC bus voltage $u_{\mathrm{dc}}$. The voltage error signal between the value of $u_{\mathrm{dc}}$ and the reference value $u_{\mathrm{dc}}^{*}$ is considered as the input of left PI regulator and the output of PI regulator which is the reference active current value $i_{\mathrm{d}}^{*}$ can be obtained for inner loop. In order to realize the unity power factor on the input side, the reference reactive current value $i_{\mathrm{q}}^{*}$ is set to 0. The voltage component can be obtained as the output of the bottom-right PI regulator after the difference between two values of $i_{\mathrm{q}}$ and $i_{\mathrm{q}}^{*}$ passing through the regulator. In Fig. 3, the currents of the two axes d and q are not completely decoupled, so the two methods of decoupling and voltage feedforward can be selected. The actual current on the d-q axes as the output of the current inner loop PI regulator can be compensated to the SPWM model by multiplying by $\omega L$. The drive signals for the devices can be generated, which can control the power electrical devices turn on and turn off.

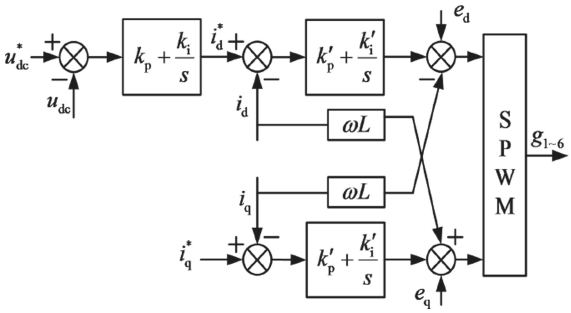


**Fig. 3.** Input portion control block diagram.

2) Controller design

Design the closed loop system in Fig. 3.

a) Inner loop controller design

The converter model in the d-q coordinate system is:

$$\begin{cases} C\dfrac{du_{dc}}{dt} = \dfrac{3}{2}(i_d S_d + i_q S_q) - \dfrac{u_{dc}}{R_L} \\ L\dfrac{di_d}{dt} + Ri_d - \omega L i_q = e_{gd} - u_{dc} s_d \\ L\dfrac{di_q}{dt} + Ri_q - \omega L i_d = e_{gq} - u_{dc} s_q \end{cases} \tag{4}$$

Where: $S$d- the d-axis switch function; $S$q- the q-axis switch function.

To effectively control the current inner loop, the current inner loop analysis should be performed first, and the Eq. (4) changes through formula variation by using the Laplace transformation:

$$Li_d(s) + Ri_d(s) - \omega L i_q(s) = e_{gd}(s) - u_{dc}(s) s_d(s) \tag{5}$$

$$Li_q(s) + Ri_q(s) - \omega L i_d(s) = e_{gq}(s) - u_{dc}(s) s_q(s) \tag{6}$$

$$Cu_{dc}(s) = \frac{3}{2}(i_d(s) S_d(s) + i_q(s) S_q(s)) - \frac{u_{dc}(s)}{R_L} \tag{7}$$

From formulas (5) and (7), the converter decoupling model can be shown in Fig. 4.

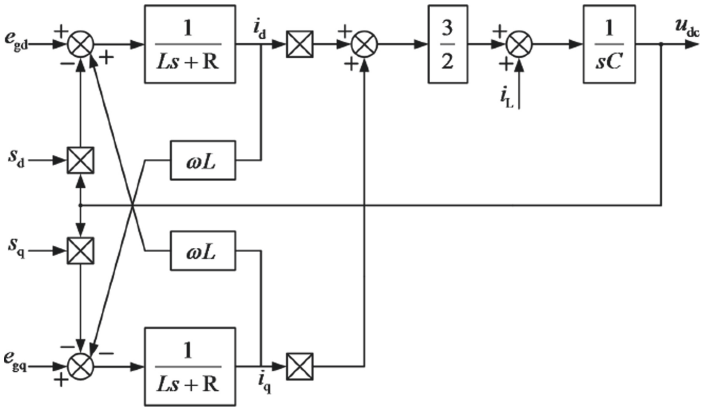


**Fig. 4.** Transformer decoupling model.

After decoupling the two axes d and q. The block diagram of the system closed-loop control is shown in Fig. 5 [22–24].

The system transfer function is:

$$G_{io}(s) = \left(\frac{1}{T_s S - \pi}\right)\left(K_p + \frac{k_i}{s}\right)\left(\frac{k_{PWM}}{0.5 T s S} + 1\right)\left(\frac{1}{Ls + R}\right) \tag{8}$$

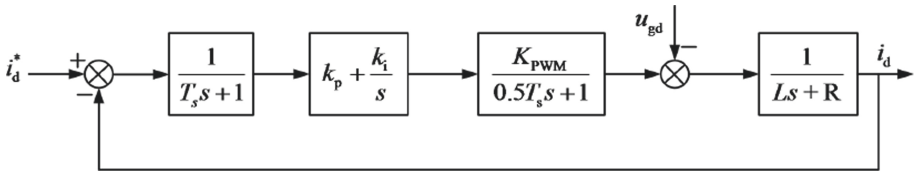


**Fig. 5.** Block diagram of closed-loop system control structure.

$k_{PWM}$- PWM gain; $T_s$- current inner loop current sampling period(s); $k_p$- current regulator scale factor; $k_i$- current regulator integral coefficient.

b) Outer loop controller design

The design of voltage conversion can be referenced [25, 26], and its block diagram is shown as Fig. 6.

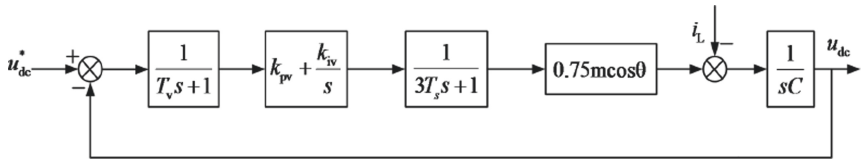


**Fig. 6.** Voltage closed-loop structure diagram.

The system transfer function is:

$$G_{vo}(s) = \left(\frac{1}{T_v S+1}\right)\left(k_{pv}+\frac{k_{iv}}{s}\right)\left(\frac{1}{3T_s S+1}\right)\left(\frac{0.75m\cos\theta}{sC}\right) \tag{9}$$

$T_v$- inertial time constant (s); $k_{pv}$- voltage regulator scale factor; $k_{iv}$- voltage regulator integral coefficient; $0.75mcos\theta$- the DC side current considering the fundamental component of the switching function; $m$-modulation ratio.

### 3.2 Control Topology of the PWM Converter on the Output Side

1) Control topology for the output side

Unlike the input portion, for the output side PWM converter, it is controlled to convert high-frequency direct current into low-voltage alternating current, which requires constant output side voltage and frequency. In order to achieve the goal, in general, the constant voltage and constant frequency control topology is selected [14] as shown in Fig. 7.

The control topology on the output side is roughly the same as on the input side and consist of two modules: the voltage outer loop and the current inner loop. The difference is that the voltage outer loop on the output side is AC. The error signal of the d and q two axes are adjusted by PI to obtain the current inner loop command value. The command

value is subtracted from the feedback value to obtain the current error signal, which is fed into the PI to get the voltage values in d and q axes [27]. Finally, the drive signals can be generated through the SPWM model.

2) Controller design

a) Inner loop controller design

The control block diagram of the inverter can be shown as in Fig. 8.

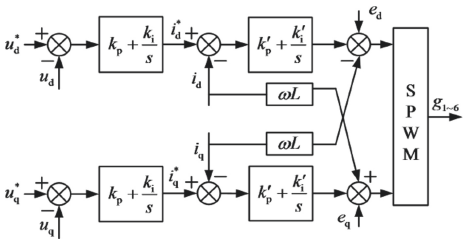


**Fig. 7.** DC-AC converter control topology.

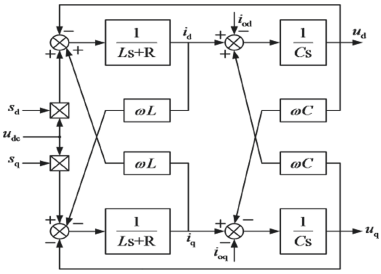


**Fig. 8.** Control block diagram of the inverter.

The structure block diagram that can be drawn from Fig. 8 as Fig. 9.

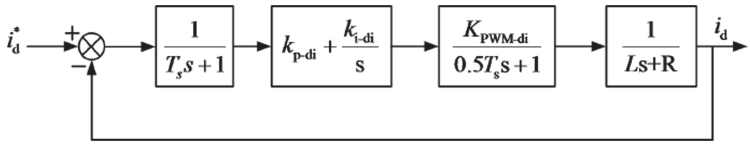

**Fig. 9.** Current closed-loop structure block.

b) Outer loop controller design

As shown in Fig. 8, the structures in d and q axes are the same with each other. So the analysis of voltage closed-loop parameters in d-axis is taken as an example. The block diagram is established as in Fig. 10.

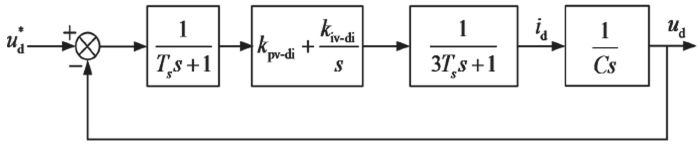


**Fig. 10.** Block diagram of voltage closed-loop transfer function at low voltage side.

## 4 Simulation Modeling and Results Analysis

### 4.1 Simulation Modeling

1) System modeling diagram

Based on the software MATLAB/Simulink, the PET system simulation model is built as shown in Fig. 11. The parameters include: the frequency of the grid (50 Hz), capacity (10 MVA), the switch frequency of output side inverter (1000 Hz), the output voltage of the inverter (660 V), the simulation time (0.3 s). And there is a load mutation (equivalent to half the load reduction) at 0.15 s.

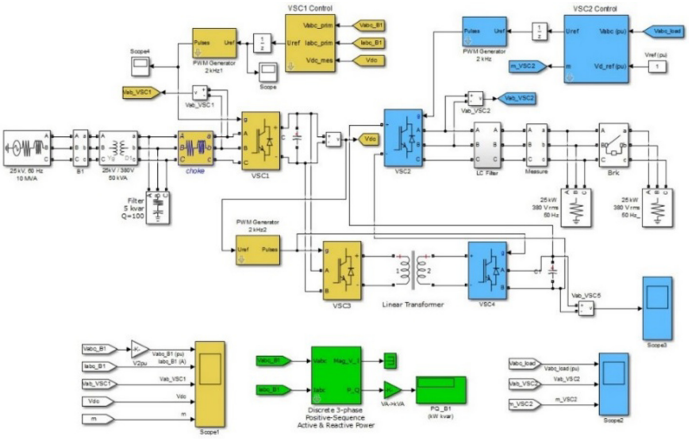


**Fig. 11.** Simulation model of PET system.

The simulation model is built as in Fig. 11. The common bridge circuit is selected as the converter circuit for rectifier and inverter on both primary side and secondary side.

Because of the high working frequency, the size and weight of the transformer are greatly reduced. The variation on the original side can be coupled to the secondary side through the intermediate isolation portion [19, 28]. A dual-loop control strategy is selected for the input and output portions. The intermediate isolation portion is implemented by open-loop control, and the gate signals are sent by the PWM Generator.

2) System control module modeling

PWM control module is shown in Fig. 12.

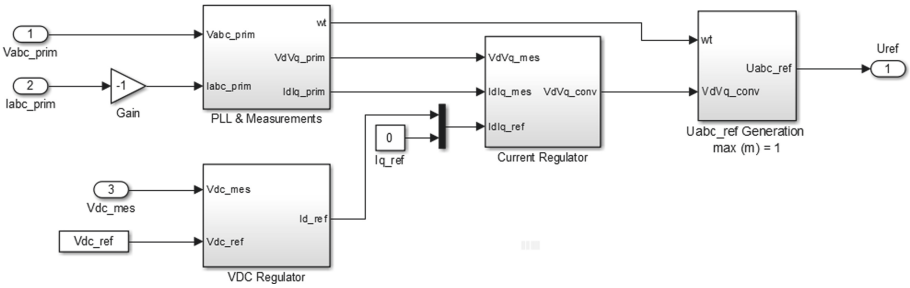


**Fig. 12.** PWM control module.

It consists of four various modules:

a) Phase-locked loop(PLL) module

The phase of the grid voltage is locked using a phase-locked loop (PLL) module. The circuit is shown in Fig. 13.

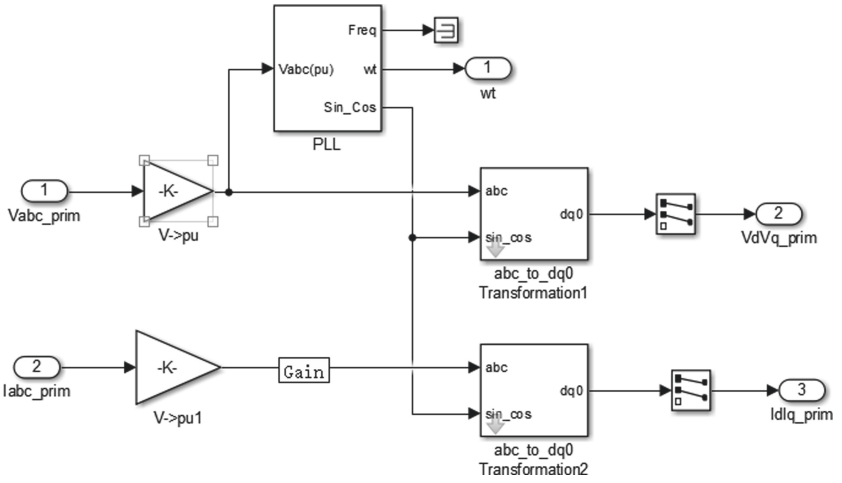


**Fig. 13.** Phase-locked loop module.

b) Voltage loop module

The voltage loop module is designed as described above shown in Fig. 14.

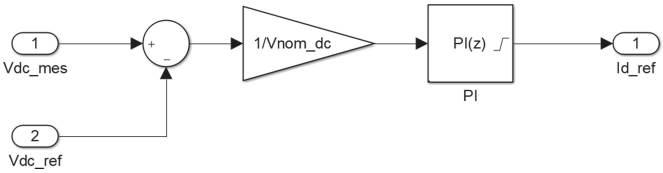


**Fig. 14.** Voltage loop module.

c) Decoupling module

As shown in Fig. 15, $i_d$ is decoupled from $i_q$ in the decoupling module constructed according to the decoupling circuit in Fig. 3.

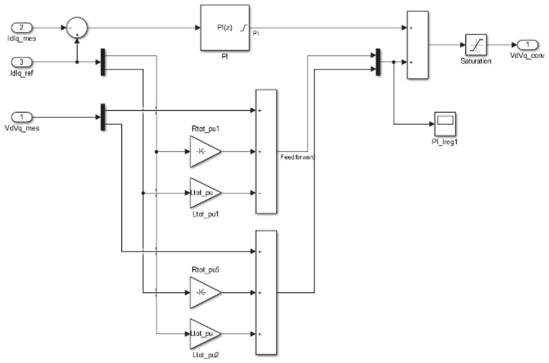

**Fig. 15.** Decoupling module.

d) PWM generation module

The PWM generation module is drawn as shown in Fig. 16.

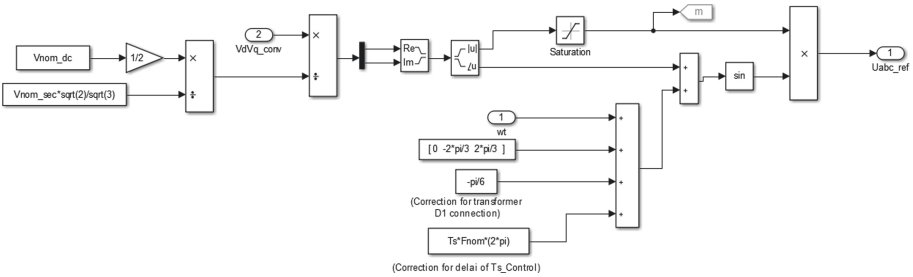


**Fig. 16.** PWM generation module.

## 4.2 Simulation Result Analysis

1) Input side simulation results

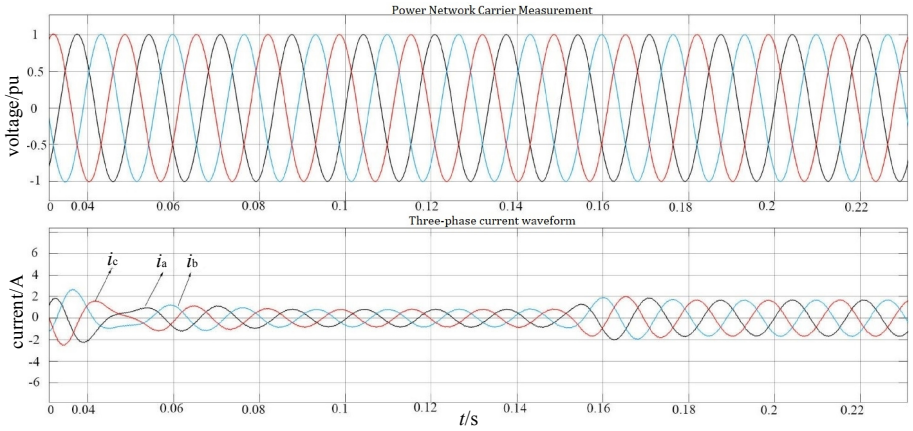


**Fig. 17.** Input side voltage and current simulation results.

The upper image in Fig. 17 shows the grid voltage per unit measurement waveforms, the value of which is obtained by the normalized three-phase voltage. And the following picture is a three-phase current graph. At 0.15 s, the load mutation occurred (parallel connection with another load module), so the current increased. In addition, it can be seen in Fig. 17, the phase of grid voltage and current are the same, even the load changes. The isolation transformer plays the role of improving the quality of electrical energy.

Figure 18 is the input line voltage waveform and the IGBT voltage waveform. From the figure the input variable is the alternating current. The DC voltage can be stabilized after rectification filtering as shown in Fig. 19. The voltage is rapidly reduced by 7.14% after a load mutation at 0.15 s (parallel connection with another load module). Due to the presence of the control system, the voltage gets back to the original voltage value after about 0.02 s.

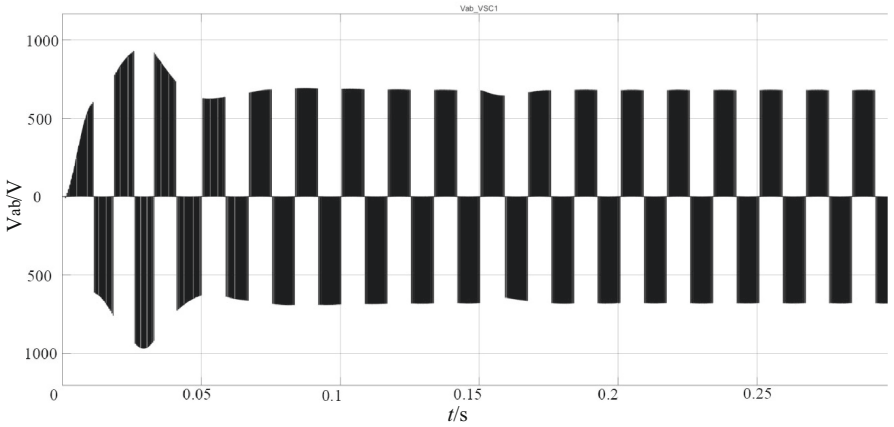


**Fig. 18.** Input line voltage.

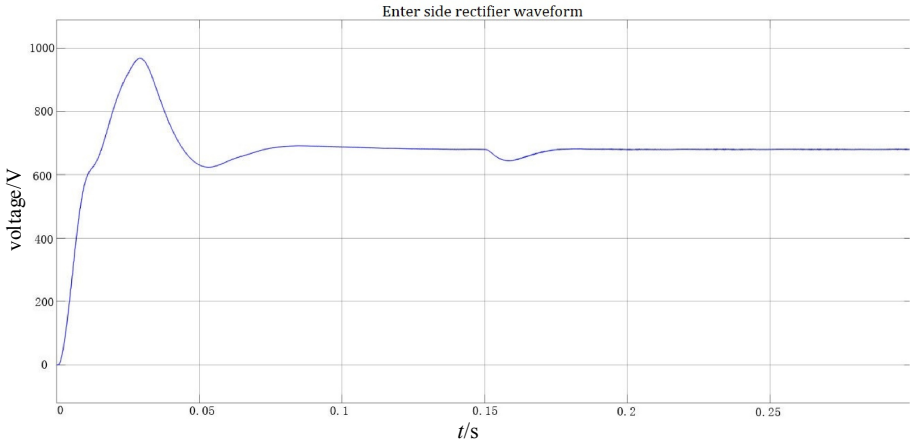


**Fig. 19.** The voltage after entering the side rectifier.

2) Isolated side simulation results

From Fig. 20, the voltage value of the output is the same as that of the rectifier output. The isolation transformer had not changed its output voltage.

3) Output side simulation results

Figure 21 is three-phase load voltage waveforms, which can quickly restore to the normal operating voltage after the load mutation. It is shown that the control system is good and the power factor of the system is approximately 1.

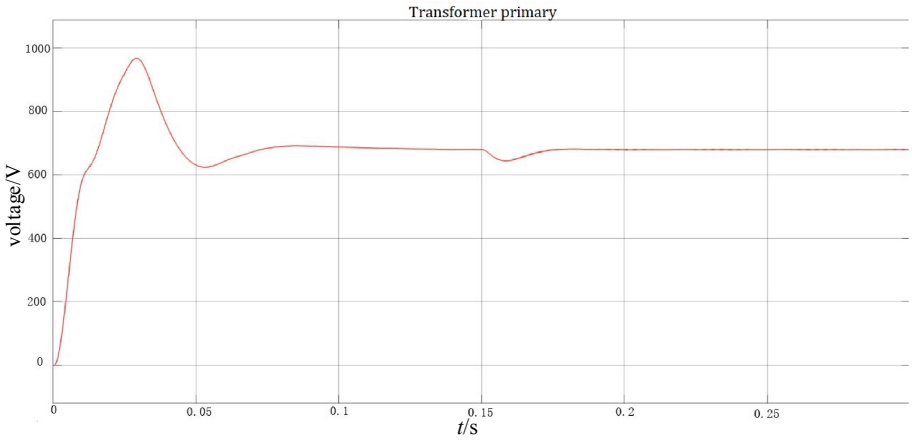


**Fig. 20.** Isolated side output voltage.

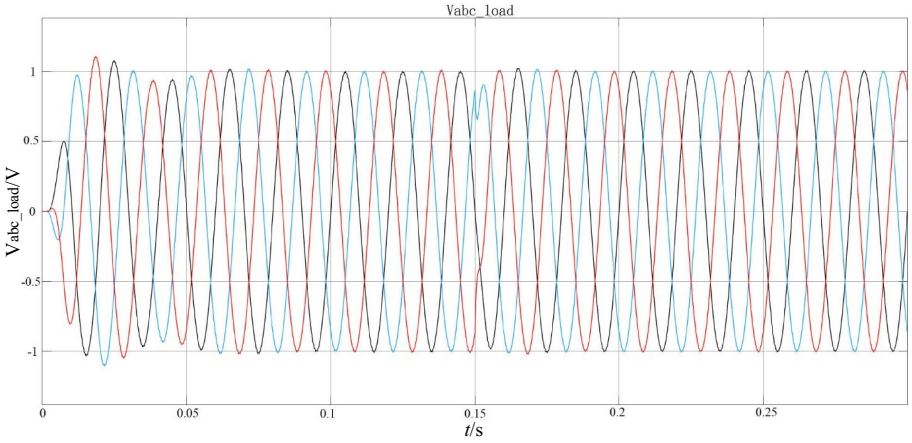


**Fig. 21.** Output side load voltage.

## 5 Conclusions

With smart substations for application, the control topologies for PETs are studied in this paper. AC/AC PET can be applied to grid-connected inverters and can also be used for power generation. DC/AC PET can be used in solar inverters while reducing the substation cost and improving the system reliability. The advantages of PET compared to traditional transformers are studied in this paper and the importance of PET for smart substations is shown.

The topological structure of input portion, isolation portion and output portion are analyzed. The converter models and control strategies are accomplished by MATLAB/Simulink.

Since the output variables of the input and output portions are different, the output variables of each portion in PET is analyzed. And the control topologies are designed for different purposes separately. The control block diagrams are given above. The correctness of the theory is proved by the simulation results of each module.

**Acknowledgements.** The authors acknowledge the Jiangsu University Natural Science Research Project (18KJB470024) and Provincial Construction System Science and Technology Project of Jiangsu Provincial Housing and Urban-Rural Construction Department (2018ZD088). This work is partly supported by the Natural Science Foundation of Jiangsu Province of China (No. BK20161165), the applied fundamental research Foundation of Xuzhou of China (No. KC17072). The authorized patents for invention are also the research and development of Jiangsu Province Industry-University-Research Cooperation Project (BY2019056).

## References

1. Wensi, L.: Research on Modeling Method and Control Technology of Power Electronic Transformer. Shandong University, Shandong (2011)
2. Yisheng, Y., Kaixiang, M., Shiying, Y.: Large signal modeling and analysis of DC-bus voltage of power electronic transformer applied in electric locomotive. Power System Protection and Control (2019)
3. Jiang, D., Wang, Y., Lv, Z., Wang, W., Wang, H.: An energy-efficient networking approach in cloud services for IIoT networks. IEEE J. Sel. Areas Commun. **38**(5), 928–941 (2020)
4. Feng, X., Jun, J.: Simulation research on improving power quality of power electronic transformer. Electromech. Inf. **36**, 4–6 (2018)
5. Jiang, D., Wang, W., Shi, L., Song, H.: A compressive sensing-based approach to end-to-end network traffic reconstruction. IEEE Trans. Netw. Sci. Eng. **7**(1), 507–519 (2020)
6. Xiang-Long, L., et al.: Coordinating voltage regulation for AC-DC hybrid distribution network with multiple power electronic transformer. Adv. Technol. Electr. Eng. Energy (2019)
7. Jiang, D., Huo, L., Song, H.: Rethinking behaviors and activities of base stations in mobile cellular networks based on big data analysis. IEEE Trans. Netw. Sci. Eng. **7**(1), 80–90 (2020)
8. Jiang, D., Wang, Y., Lv, Z., Qi, S., Singh, S.: Big data analysis based network behavior insight of cellular networks for industry 4.0 applications. IEEE Trans. Ind. Inform. **16**(2), 1310–1320 (2020)
9. Jiang, D., Huo, L., Lv, Z., Song, H., Qin, W.: A joint multi-criteria utility-based network selection approach for vehicle-to-infrastructure networking. IEEE Trans. Intell. Transp. Syst. **19**(10), 3305–3319 (2018)
10. Tian, Z.: Design of Power Electronic Transformer. Ind. Control Comput. **30**(12), 149–150 (2017)
11. Jiang, D., Huo, L., Li, Y.: Fine-granularity inference and estimations to network traffic for SDN. PLoS ONE **13**(5), 1–23 (2018)
12. Lewicki, A., Morawiec, M.: The structure and the space vector modulation for a medium voltage power-electronic-transformer based on two seven-level cascade H-bridge inverters. IET Electric Power Appl. **13**(10), 1514-1523 (2019)
13. Wang, Y., Jiang, D., Huo, L., Zhao, Y.: A new traffic prediction algorithm to software defined networking. Mob. Netw. Appl. 110 (2019)
14. Zhang, X.: Research on PWM rectifier and its control strategy. Ph.D. Thesis, Hefei University of Technology (2003)

15. Qi, S., Jiang, D., Huo, L.: A prediction approach to end-to-end traffic in space information networks. Mob. Netw. Appl. 110 (2019)
16. Shaodi, O., et al.: DC voltage control strategy of three-terminal medium-voltage power electronic transformer-based soft normally open points. IEEE Trans. Ind. Electron. **67**(5), 3684-3695 (2019)
17. Jiang, D., Zhang, P., Lv, Z., et al.: Energy-efficient multi-constraint routing algorithm with load balancing for smart city applications. IEEE Internet Things J. **3**(6), 1437–1447 (2016)
18. Jiang, D., Li, W., Lv, H.: An energy-efficient cooperative multicast routing in multi-hop wireless networks for smart medical applications. Neurocomputing **2017**(220), 160–169 (2017)
19. Qin, H., Kimbal, J.W.: Solid-state transformer architecture using AC–AC dual-active-bridge converter. IEEE Trans. Ind. Electron. **60**(9), 3720–3730 (2013)
20. Yang, Y., Pei, W., Deng, W., et al.: Benefit analysis of using multi-port and multi-function power electronic transformer connecting hybrid AC/DC power grids. J. Eng. **2019**(16), 1076–1080 (2019)
21. Li, J.: Discussion on the control and application of electronic power transformer. Heilongjiang Sci. Technol. Inf. (23), 53 (2016)
22. Wang, F., Jiang, D., Qi, S.: An adaptive routing algorithm for integrated information networks. China Commun. **7**(1), 196–207 (2019)
23. Geng, Q., Hu, Y.: Energy storage device locating and sizing based on power electronic transformer. J. Eng. **2019**(16), 3164–3168 (2019)
24. Huo, L., et al.: An AI-based adaptive cognitive modeling and measurement method of network traffic for EIS. Mob. Netw. Appl. 110 (2019)
25. Huo, L., Jiang, D., Lv, Z., et al.: An intelligent optimization-based traffic information acquirement approach to software-defined networking. Comput. Intell. **36**(1), 151-171 (2019)
26. Zhao, J.: Simulation of power electronic transformer with constant output voltage. Power Syst. Autom. **27**(18), 30-33 (2003)
27. Guo, S., Mu, Y., Jia, H., et al.: Optimization of AC/DC hybrid distributed energy system with power electronic transformer. Energy Procedia **158**, 6687–6692 (2019)
28. Liu, Z., Lin, Y.: Design and simulation of power electronic transformer in distributed power generation system. Electr. Appl. **37**(06), 82–86 (2008)